

r-Process and Kilonovae

Shinya WANAJO^{1,2,3}

¹*Max-Planck-Institut für Gravitationsphysik (Albert-Einstein-Institut), Am Mühlenberg 1, D-14476 Potsdam-Golm, Germany*

²*RIKEN iTHEMS Research Group, 2-1 Hirosawa, Wako, Saitama 351-0198, Japan*

³*Department of Engineering and Applied Sciences, Faculty of Science and Technology, Sophia University, 7-1 Kioicho, Chiyoda-ku, Tokyo 102-8554, Japan*

E-mail: shinya.wanajo@aei.mpg.de

(Received September 13, 2019)

The kilonova associated with the neutron star merger GW170817 provides us with several hints to elucidate the nature of the *r*-process in the universe. In this article, we inspect the radioactive isotopes that powered the kilonova emission, provided that the merger ejecta consisted of material with a solar *r*-like abundance pattern. It is suggested that the early (1–10 days after merger) kilonova emission is mainly due to the β -decay chain $^{66}\text{Ni} \rightarrow ^{66}\text{Cu} \rightarrow ^{66}\text{Zn}$, which can be the source of the steepening of the light curve at about 7 days. The late time (> 10 days) heating is attributed to the α -decay and fission (^{254}Cf) of trans-Pb species (in addition to β -decay), which can be the signature of *r*-processing beyond the heaviest stable elements. This article summarizes a recent work by the author [1] with the additional calculations of kilonova light curves by using a numerical code in [2].

KEYWORDS: nucleosynthesis, neutron star mergers, kilonovae, *r*-process

1. Introduction

The discovery of a kilonova [3, 4], the electromagnetic counterpart of the gravitational wave signal from the neutron star merger GW170817 [5], gives us a unique opportunity to directly inspect the *r*-process nucleosynthesis in the universe. The luminosity of the kilonova indicates the ejecta mass of $M_{\text{ej}}/M_{\odot} = 0.03\text{--}0.06$ [6–9], which points an ejection of material from the post-merger accretion disk [10–16] in addition to the early dynamical ejecta [17–23]. Its spectral evolution suggests the lanthanide mass fraction of $X_{\text{lan}} = 0.001\text{--}0.01$ [7, 24–26], which confirms the production of the heavy elements with $Z \geq 57$ ($A \geq 139$). An identification of Sr has recently been reported by inspection of the highly Doppler-shifted spectra of the kilonova ejecta [27]. Nevertheless, an evidence of the production of the heaviest *r*-process elements such as gold and uranium is still missing. Furthermore, no information of the nucleosynthetic abundance distribution has been obtained, which in fact determines the radioactive heating rate for the kilonova emission. Here we try to identify the dominant radioactive species that powered the kilonova emission of the merger GW170817. The merger ejecta are assumed to be composed of material with a solar *r*-like abundance pattern, in light of the spectroscopic study of *r*-enhanced stars in the Milky Way (MW) halo [28]. This article summarizes the work in [1] with updates by including the kilonova light curves computed with a numerical code in [2].

2. Models and nucleosynthesis

Thermodynamic histories of the ejecta are obtained from a free expansion model (FE) [1], in which the density and temperature are calculated from a suite of three parameters, i.e., expansion velocity (v), initial entropy (S ; in units of Boltzmann constant per nucleon), and initial electron frac-

Table I. Mass fractions (in units of %) of lanthanides and those of radioactive isotopes at 0.1 days.

Model	A_{\min}	lanthanide	^{66}Ni	^{72}Ge	^{127}Sn	^{132}I	^{222}Rn	^{223}Ra	^{224}Ra	^{225}Ra	^{254}Cf
mFE-a	69	1.4	2.6	0.66	0.28	0.27	0.0095	0.010	0.0057	0.017	0.0040
mFE-b	88	8.6	0.30	0.14	1.8	1.6	0.057	0.061	0.035	0.10	0.026

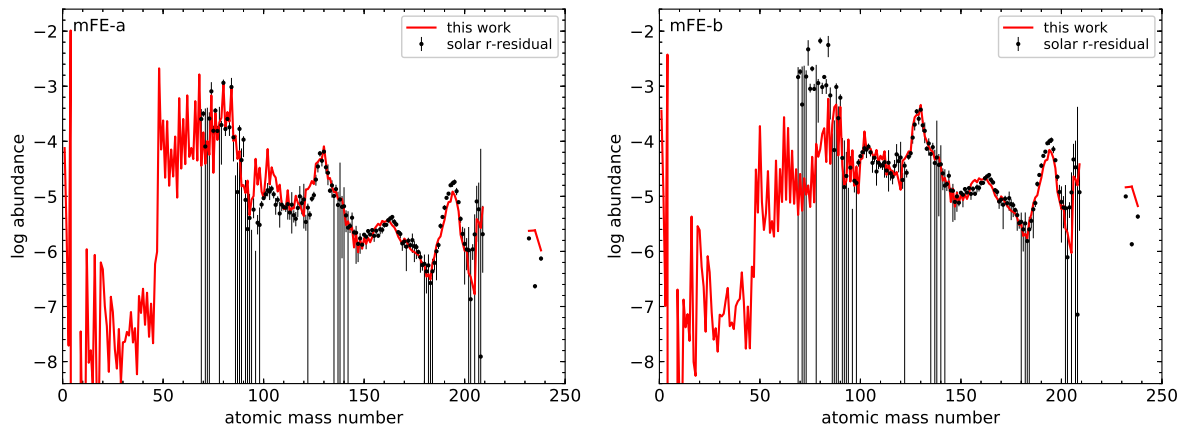


Fig. 1. Final nuclear abundances (red lines) for mFE-a (left) and mFE-b (right). The black circles (with error bars) indicate the r -residuals to the solar abundances [29], which are vertically shifted to match the abundances at $A = 138$.

tion (Y_e). The adopted ranges of parameters are $(v/c, S, Y_e) = (0.05-0.30, 10-35, 0.01-0.50)$ with the intervals $(\Delta v/c, \Delta S, \Delta Y_e) = (0.05, 5, 0.01)$, 1800 FEs in total, which cover those predicted from the recent hydrodynamical simulations of neutron star mergers. Temporal evolution of 6300 isotopes for each FE is computed by using an up-to-date reaction network code described in [1].

In this study, we assume that the ejecta from a neutron star merger compose of material with a solar r -like abundance pattern, according to the spectroscopic studies of r -enhanced stars in the MW halo [28]. The r -residuals to the solar system abundances in [29] are taken to be reference for this purpose. Two cases with different minimum A are considered: a) $A_{\min} = 69$ and b) $A_{\min} = 88$ (Table I). The reason for these choices is twofold. First is due to few measurements of elements lighter than Sr ($A = 88$) in MW halo stars (except for Ga and Ge in several stars based on only single lines) [28, 30]. Second is that the isotopes with $A < 88$ can be made in nuclear statistical equilibrium (NSE) or nuclear quasi-equilibrium (QSE), a different condition from an r -process [31–33]. For both cases, the maximum A is taken to be $A_{\max} = 205$ because of large uncertainties in the r -residuals of Pb and Bi (Fig. 1). Radioactive species Th and U are not included, either.

For each case, a multi-component FE (mFE) is constructed by fitting a linear combination of all FEs to the r -residuals. The final abundance distributions (after decay) are in reasonable agreement with those of the r -residuals between A_{\min} and A_{\max} for both cases (mFE-a and mFE-b), as can be seen in Fig. 1. Moreover, we find that the nuclei with $A < A_{\min}$ and $A > A_{\max}$ are co-produced: Fe-group (for mFE-a) and trans-Pb nuclei. For mFE-a, the isotopes with $A = 48-68$ are made with the first-peak abundances of r -residuals ($A \sim 80$) under similar physical conditions (NSE or QSE). The resultant mass fractions of lanthanides for mFE-a and mFE-b are $X_{\text{lan}} = 0.014$ and 0.086 (Table I), respectively. The former (mFE-a) is in marginal agreement with the inferred value for the kilonova of the merger GW170817; the latter (mFE-b) is too large to be a reasonable model for this event.

3. Radioactive heating rates

The heating rates from the decays of radioactive isotopes are computed for each case (mFE-a or mFE-b) as an ensemble of those in all FEs. The resulting mass fractions of several important radioactive isotopes at 0.1 days are listed in Table I.

3.1 β -decay

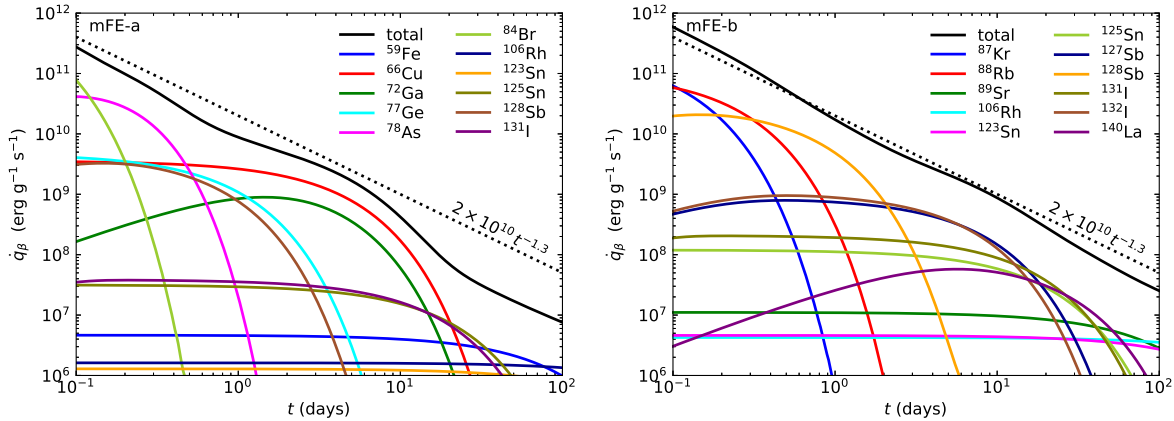


Fig. 2. Heating rates from the β -decays of dominant contributors (solid lines with different colors) for mFE-a (left) and mFE-b (right). The black solid and dotted lines indicate the total heating rate from β -decay and the empirical (power-law) rate, respectively.

The heating rates from β -decay are shown in Fig. 2, where the total and individual rates are indicated by black and colored lines, respectively. On the one hand, for mFE-b, the total heating rate from β -decay approximately follows the power law as suggested in previous works [20, 34] because of the contribution of a number of isotopes around the second peak ($A \sim 130$) with different half-lives. On the other hand, for mFE-a, the total heating rate exhibits a bump at several days, because of the dominant decay chain ^{66}Ni (2.28 d) \rightarrow ^{66}Cu (5.12 m) \rightarrow ^{66}Zn and in part ^{72}Zn (1.94 d) \rightarrow ^{72}Ga (14.1 h) \rightarrow ^{72}Ge ; the power law cannot be taken as an approximation for this case. It should be noted that, for both mFE-a and mFE-b, these results are robust because of the experimentally evaluated half-lives and decay energies for the relevant isotopes (close to the β -stability).

3.2 α -decay and fission

Spontaneous fission and α -decay of trans-Pb isotopes are suggested to be the heating sources of a kilonova at late times (> 10 days) [1, 20, 35–37]. Fig. 3 displays the nuclear abundances of trans-Pb species at different times for mFE-a and mFE-b, both of which exhibit almost the same abundance patterns but with different amounts (about 6 times greater for mFE-b). We find that the distribution extends to $A = 266$ including several Cf and Fm isotopes. It should be noted that the distribution of trans-Pb isotopes as well as the maximum A is highly sensitive to the nuclear inputs such as the masses and fission barriers [38, 39].

Fig. 4 shows the total and individual heating rates from α -decay and fission for mFE-a; those for mFE-b are almost the same except for their 6 times greater values. The relatively longer half-lives of dominant contributors than those for β -decay make their role important at late times (> 10 days) [20, 35, 39]. We find from Fig. 4 (left) that the four α -decay chains (starting from those in Table I) play dominant roles at late times [2, 37]: ^{222}Rn (3.82 d) \rightarrow ^{218}Po (3.10 m) \rightarrow ^{214}Pb (26.8 m) \rightarrow ^{214}Bi (19.9 m) \rightarrow ^{214}Po (164 μs) \rightarrow ^{210}Pb (22.2 yr) \rightarrow ^{210}Bi (5.01 d) \rightarrow ^{206}Tl (4.20 m) \rightarrow ^{206}Pb , ^{223}Ra (11.4 d) \rightarrow ^{219}Rn (3.96 s) \rightarrow ^{215}Po (1.78 ms) \rightarrow ^{211}Pb (36.1 m) \rightarrow ^{211}Bi (2.14 m) \rightarrow ^{207}Tl (4.77 m)

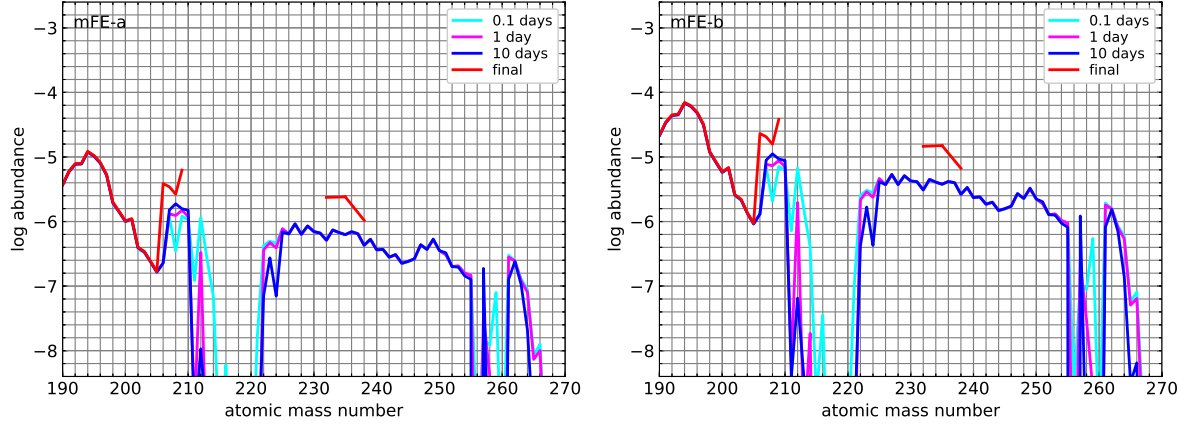


Fig. 3. Final nuclear abundances for $A \geq 190$ (red) along with those at 0.1 days (cyan), 1 day (magenta), and 10 days (blue).

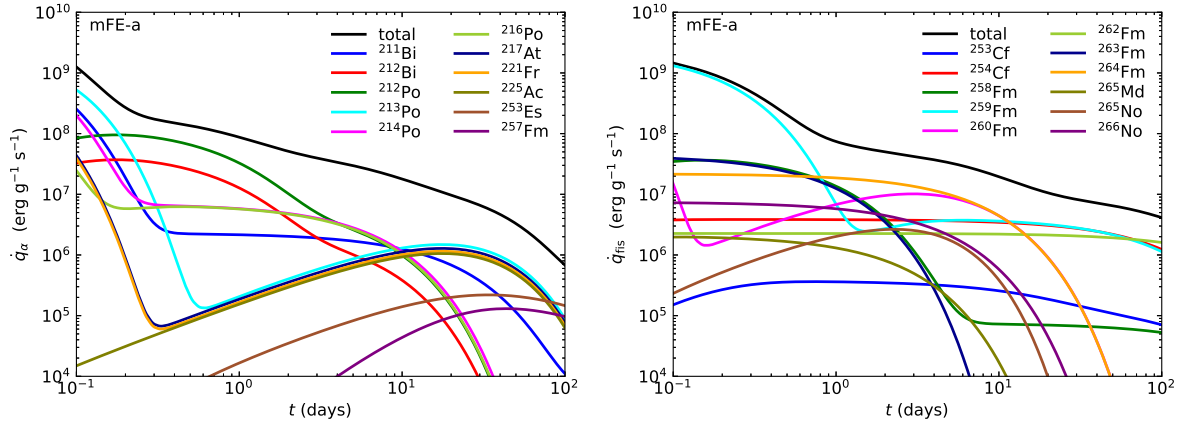


Fig. 4. Heating rates from the α -decay (left) and fission (right) of dominant contributors (solid lines with different colors) for mFE-a. The black solid line indicates the total heating rate for each decay channel.

$\rightarrow {}^{207}\text{Pb}$, ${}^{224}\text{Ra}$ (3.66 d) $\rightarrow {}^{220}\text{Rn}$ (55.6 s) $\rightarrow {}^{216}\text{Po}$ (145 ms) $\rightarrow {}^{212}\text{Pb}$ (10.6 h) $\rightarrow {}^{212}\text{Bi}$ (1.01 h) $\rightarrow {}^{208}\text{Tl}$ (3.05 m) $\rightarrow {}^{208}\text{Pb}$, and ${}^{225}\text{Ra}$ (14.9 d) $\rightarrow {}^{225}\text{Ac}$ (10.0 d) $\rightarrow {}^{221}\text{Fr}$ (4.77 m) $\rightarrow {}^{217}\text{At}$ (32.3 ms) $\rightarrow {}^{213}\text{Bi}$ (45.6 m) $\rightarrow {}^{213}\text{Po}$ (3.72 μs) $\rightarrow {}^{209}\text{Pb}$ (3.25 h) $\rightarrow {}^{209}\text{Bi}$. For spontaneous fission, ${}^{254}\text{Cf}$ (with the half-life 60.5 days) and a few Fm isotopes become dominant contributors at late times. The reason for the contribution of Fm isotopes with very short half-lives (e.g., 1.5 s for ${}^{259}\text{Fm}$) at late times is due to the theoretically predicted (relatively long) β -decay half-lives along their isobars.

4. Kilonova light curves

The kilonova light curves for mFE-a and mFE-b are computed by using the numerical code described in [2] (Fig. 5). The ejecta masses are taken to be $M_{\text{ej}}/M_{\odot} = 0.07$ and 0.06, respectively, so that the light curve matches the inferred bolometric luminosities of the kilonova between 1 day and 10 days after merger (GW170817) [26] (see the figure caption for other parameters). For α -decay, the four decay chains from ${}^{222}\text{Rn}$, ${}^{223}\text{Ra}$, ${}^{224}\text{Ra}$, and ${}^{225}\text{Ra}$ (Table I) are included. For spontaneous fission, only ${}^{254}\text{Cf}$ (Table I) is considered, because the contribution of other (Fm) isotopes is owing to the highly uncertain β -decay half-lives that are theoretically predicted (although such a possibility cannot be excluded).

We find that, when only β -decay is included (dashed line), both mFE-a and mFE-b give consistent results with the kilonova luminosity between 1 day and 15 days (circles with error bars). The former (mFE-a) is still in agreement with the observation when including the contributions of α -decay (dot-

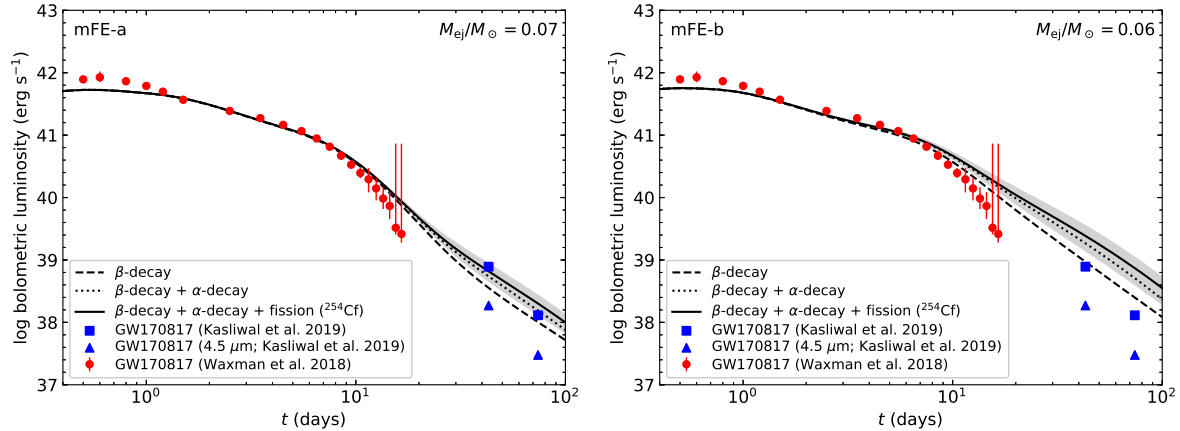


Fig. 5. Light curves for mFE-a (left) and mFE-b (right) computed with the numerical code in [2]. The assumed ejecta masses are $M_{\text{ej}}/M_{\odot} = 0.07$ and 0.06 , respectively. For the radial density profile of the ejecta, Eq. (12) in [2], $v_0/c = 0.1$, $v_{\text{max}}/c = 0.4$, and $n = 4.5$ are adopted. The opacities (in units of $\text{cm}^2 \text{g}^{-1}$) in mFE-a and mFE-b are chosen to be, respectively, 0.3 and 0.5 for $v > v_{\kappa}$ and 0.3 (same for both cases) for $v/c < v_{\kappa}$, where $v_{\kappa}/c = 0.14$ and 0.20 . The solid line indicates the bolometric luminosity (erg g^{-1}) as a function of time (days), in which all the decay channels (β -decay, α -decay, and fission) are included. The gray shaded region brackets the range of the light curve owing to the variation of trans-Pb abundances (see text). The dotted and dashed lines are those without fission (β -decay and α -decay) and without the contribution of trans-Pb nuclei (β -decay only). Here ^{254}Cf is taken as the exclusive source of the fission channel. The red circles (with error bars) are the bolometric luminosities of the kilonova associated with GW170817 [26]. The blue triangles and squares are, respectively, the luminosities at $4.5 \mu\text{m}$ and the inferred bolometric luminosities at 43 days and 74 days after merger [40].

ted line) and fission (solid line). However, mFE-b overpredicts the luminosity at 10-15 days when α -decay and fission are considered. The measurements at 43 days and 74 days in infrared ($4.5 \mu\text{m}$; triangles) [40], placing the lower limits to the bolometric luminosities, are consistent with both cases. The inferred bolometric luminosities (squares) by [40], which should be taken with a caution (estimated from only a single band; $4.5 \mu\text{m}$), also are in reasonable agreement with mFE-a (when α -decay and fission are included) and mFE-b (when only β -decay is considered).

As noted in § 3.2, the abundance distribution of trans-Pb isotopes and thus their contribution to the heating are highly sensitive to the inputs of nuclear data. Therefore, we consider a possible range of the bolometric luminosity at late times as what follows (see [1] for more detail). We can obtain a constraint to the range of the ratio Th/Eu from the spectroscopic studies of MW halo stars (and those in the ultra-faint dwarf Reticulum II; 24 stars in total [41]) among r -enhanced stars. Th and Eu are taken to be representative of trans-Pb and lighter elements, respectively. The gray shaded region in Fig. 5 represents the obtained range of the bolometric luminosity when the ratio of trans-Pb/Eu is scaled to Th/Eu. The overprediction of the light curve at 10-15 days in mFE-b is still evident when the range of the trans-Pb production is considered, while that in mFE-a is in agreement with the observation.

5. Summary

We have inspected the radioactive isotopes that dominantly powered the kilonova associated with the neutron star merger GW170817 by using free expansion models described in [1]. The ejecta were assumed to be composed of a) NSE/QSE products ($A = 48-87$) + r -process elements ($A \geq 88$) and b) r -process elements only ($A \geq 88$). The former case (mFE-a) is in good agreement with the inferred mass fraction of lanthanides as well as the light curve of the kilonova (including its steepening at about 7 days), while the latter (mFE-b) disagrees with these observational indications.

It is concluded, therefore, the dominant heating source at early times (1-10 days) was the β -decay chain from ^{66}Ni (and in part, that from ^{72}Zn) according to the results for mFE-a. Provided that the Th/Eu ratio was between the range inferred from r -enhanced stars, α -decay and spontaneous fission (^{254}Cf) substantially contributed to the late time (> 10 days) heating, which could be a signature of the heaviest r -element production in the neutron star merger GW170817.

The author thanks Kenta Hotokezaka for useful discussion and his numerical code that was used to calculate the kilonova light curves. The author also thanks the Yukawa Institute for Theoretical Physics at Kyoto University for fruitful discussions during the workshops YITP-T-18-06 “Nucleosynthesis and electromagnetic counterparts of neutron-star mergers” and YITP-T-19-04 “Multi-Messenger Astrophysics in the Gravitational Wave Era”, which were useful to complete this work. This work was supported by the RIKEN iTHEMS Project.

References

- [1] S. Wanajo, *ApJ* **868**, 65 (2018).
- [2] K. Hotokezaka and E. Nakar, arXiv:1909.02581 (2019).
- [3] D. A. Coulter, R. J. Foley, C. D. Kilpatrick, et al., *Science* **358**, 1556 (2017).
- [4] S. Valenti, D. J. Sand, S. Yang, et al., *ApJL* **848**, L24 (2017).
- [5] B. P. Abbott, R. Abbott, T. D. Abbott, et al., *PRL* **119**, 161101 (2017).
- [6] P. S. Cowperthwaite, E. Berger, V. A. Villar, et al., *ApJL* **848**, L17 (2017).
- [7] M. Nicholl, E. Berger, D. Kasen, et al., *ApJL* **848**, L18 (2017).
- [8] M. Tanaka, Y. Utsumi, P. A. Mazzali, et al. *PASJ* **69**, 102 (2017).
- [9] K. Kawaguchi, M. Shibata, and M. Tanaka, *ApJL* **865**, L21 (2018).
- [10] L. Dessart, C. Ott, A. Burrows, S. Rosswog, and E. Livne, *ApJ* **690**, 1681 (2009).
- [11] B. D. Metzger and R. Fernández, *MNRAS* **441**, 3444 (2014).
- [12] O. Just, A. Bauswein, R. A. Pulpillo, S. Goriely, and H.-T. Janka, *MNRAS* **448**, 541 (2014).
- [13] J. Lippuner, R. Fernández, L. F. Roberts, et al., *MNRAS* **472**, 904 (2017).
- [14] M. Shibata, S. Fujibayashi, K. Hotokezaka, et al., *PRD* **96**, 123012 (2017).
- [15] D. Siegel and B. D. Metzger, *PRL* **119**, 1102 (2017).
- [16] S. Fujibayashi, K. Kiuchi, N. Nishimura, Y. Sekiguchi, and M. Shibata, *ApJ* **860**, 64 (2018).
- [17] C. Freiburghaus, S. Rosswog, and F.-K. Thielemann, *ApJL* **525**, L121 (1999).
- [18] S. Goriely, A. Bauswein, and H.-T. Janka, *ApJL* **738**, L32 (2011).
- [19] A. Bauswein, S. Goriely, and H.-T. Janka, *ApJ* **773**, 78 (2013).
- [20] S. Wanajo, Y. Sekiguchi, N. Nishimura, et al., *ApJL* **789**, L39 (2014).
- [21] Y. Sekiguchi, K. Kiuchi, K. Kyutoku, and M. Shibata, *PRD* **91**, 064059 (2015).
- [22] Y. Sekiguchi, K. Kiuchi, K. Kyutoku, M. Shibata, and K. Taniguchi, *PRD* **93**, 124046 (2016).
- [23] D. Radice, A. Perego, K. Hotokezaka, et al., *ApJ* **869**, 130 (2018).
- [24] I. Arcavi, G. Hosseinzadeh, D. A. Howell, et al., *Nature* **551**, 64 (2017).
- [25] R. Chornock, E. Berger, D. Kasen, et al., *ApJL* **848**, L19 (2017).
- [26] E. Waxman, E. O. Ofek, D. Kushnir, and A. Gal-Yam, *MNRAS* **481**, 3423 (2018).
- [27] D. Watson¹, C. J. Hansen, J. Selsing, et al., *Nature* **574**, 497 (2019).
- [28] J. J. Cowan, C. Sneden, J. E. Lawler, et al., arXiv:1901.01410 (2019).
- [29] S. Goriely, *A&A* **342**, 881 (1999).
- [30] S. Siqueira Mello Jr., M. Spite, B. Barbuy, et al., *A&A* **550**, A122 (2013).
- [31] D. Hartmann, S. E. Woosley, and M. F. El Eid, *ApJ* **297**, 837 (1985).
- [32] B. S., Meyer, T. D., Krishnan, and D. D. Clayton, *ApJ* **498**, 808 (1998).
- [33] S. Wanajo, B. Müller, H.-T. Janka, and A. Heger, *ApJ* **852**, 40 (2018).
- [34] B. D. Metzger, G. Martínez-Pinedo, S. Darbha, et al., *MNRAS* **406**, 2650 (2010).
- [35] K. Hotokezaka, S. Wanajo, M. Tanaka, et al., *MNRAS* **459**, 35 (2010).
- [36] Y. Zhu, R. T. Wollaeger, N. Vassh, et al., *ApJL* **863**, L23 (2018).
- [37] M.-R. Wu, J. Barnes, G. Martínez-Pinedo, and B.D. Metzger, *PRL* **122**, 062701 (2019).
- [38] S. Goriely, *EPJA* **51**, 22 (2015).
- [39] J. Barnes, D. Kasen, M.-R. Wu, and G. Martínez-Pinedo, *ApJ* **829**, 110 (2016).
- [40] M. M. Kasliwal, D. Kasen, R. M. Lau, et al., *MNRAS*, in press (2019).
- [41] E. M. Holmbeck, T. C. Beers, I. U. Roederer, et al., *ApJL* **859**, L24 (2018).